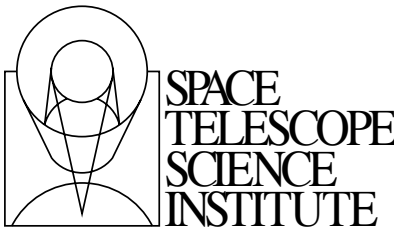

Operated for NASA by AURA

Instrument Science Report WFC 2013-03

WFC3/UVIS EPER CTE Measurement: Cycles 19 & 20

M. Bourque & V. Kozhurina-Platais

February 15, 2013

Abstract

We present WFC3/UVIS Charge Transfer Efficiency (CTE) results based on internal data acquired during Cycles 17 through the first three observations of Cycle 20, covering August 2009 through January 2013. CTE analysis was performed using the Extended Pixel Edge Response (EPER) technique, in which a special readout mode is employed and overscan pixels are used to measure the deferred charge as signal is transferred away from the science pixels. A power-law relationship between the CTE and signal level is evident. Results indicate that the CTE continues to linearly decline over time and CTE losses are strongest at the lowest signal level of ∼160 e^-.

Introduction

The HST Wide Field Camera 3 (WFC3) is a fourth-generation imaging instrument that was installed during Servicing Mission 4 in May 2009. It is recognized that all HST CCDs experience Charge Transfer Efficiency (CTE) loss, which includes ACS (Riess 2003; Mutchler & Siriani 2005), STIS (Gilliland et al. 1999, Goudfrooij & Kimble 2003; Goudfrooij et al. 2006), and WFPC2 (Whitemore et al. 1999, Dolphin 2000). CTE losses are degradations in the CCD detector performance over time and are due to cosmic rays damaging the silicon lattice. CTE losses have detrimental effects on the precision of stellar photometry and astrometry on HST science programs (Riess & Mack 2004; Kozhurina-Platais et al. 2007; Chiaberge et al. 2009).

WFC3 is no exception, and the CTE losses of the WFC3/UVIS CCD have also been documented. Kozhurina-Platais et al. (2011) (WFC3 ISR 2011-06; hereafter "A") describe a CTE evaluation based on external measurements of the rich open cluster NGC 6791, wherein the Charge Transfer Inefficiency (CTI) increased from 2% to 7% over the course of a year for the low-sky background ($\sim$ 0.1 - $\sim$ 1.0 e^-) and the flux range from 500 to 2000 e^-. Another NGC 6791 study, performed by Noeske et al. (2012), shows that CTE losses reach 0.3 mag (24%) for stars with 1000 e^- flux in zero sky background images. Furthermore, Kozhurina-Platais et al. (2011) (WFC3 ISR 2011-17; hereafter "B") describe the results from an internal study for data acquired during Cycles 17 and 18, as described below. For the latest updates on the WFC3/UVIS CTE and mitigation reccomendations, see http://www.stsci.edu/hst/wfc3/ins_performance/CTE/.

Extended Pixel Edge Response (EPER), described by Janesick (2001), is a popular technique to measure the loss of CTE on various CCD detectors. The EPER technique aims to measure the profiles of excess charge in the overscan pixels (also known as the extended pixel region) of the CCD. This excess charge decreases exponentially with distance from the science pixels. The EPER technique has been widely used to measure the CTE, such as for the ACS Wide Field Camera (WFC) and High Resolution Camera (HRC) (Mutchler & Sirianni 2005), for WFC3/UVIS-2 during the ground-based ambient test (Robberto 2007), and for the WFC3/UVIS flight detector during ground-based thermal vacuum tests (Kozhurina-Platais et al. 2009). In addition, Kozhurina-Platais et al. (2011 B) describe internal EPER CTE measurements for WFC3/UVIS through Cycles 17 and 18. They report that the CTE declines linearly with time at signal levels ranging from $\sim$160 e^- to $\sim$5000 e^-.

In this paper, we present the results of on-orbit internal WFC3/UVIS EPER observations performed during Cycle 19, as well as the first three observations from Cycle 20, supplementing the data described in Kozhurina-Platais (2011 B). Thus, this paper serves as an update to their UVIS EPER CTE measurements.

UVIS EPER Observations

Observations were performed through programs CAL-11924 (Cycle 17, PI Kozhurina-Platais), CAL-12347 (Cycle 18, PI Kozhurina-Platais), CAL-12691 (Cycle 19, PI Kozhurina-Platais), and CAL-13082 (Cycle 20, PI Bourque). Each program is comprised of 24 internal orbits with observations of tungsten lamp flat fields, grouped in pairs of visits. Each visit pair covers tungsten flat field observations in several filters for an extensive range of illumination levels, as shown in Table 1. Since the Flight Software does not allow bias exposures (i.e. an exposure time of 0 seconds) in EPER mode, short dark exposures are used as a bias.

Visit	Type	Filter	Exp. Time (sec)	Intended Illumination Level (e^-/pix)
n	DARK	—	0.5	—
n	TUNGSTEN	F390M	9.2	200
n	TUNGSTEN	F390M	22.9	400
n+1	DARK	—	0.5	—
n+1	TUNGSTEN	F390W	6.4	800
n+1	TUNGSTEN	F438W	7.6	1600
n+1	TUNGSTEN	F438W	22.7	5000

Table 1: *Observational parameters for a two-visit pair, where n is the first visit in the series and n+1 is the second.*

Data were collected through a special EPER detector format and readout mode. Under normal circumstances, the WFC3 UVIS CCD detectors, each of size 4096 × 2051 pixels, have a serial physical overscan region consisting of 25 reserved columns on each side of the detector. In addition, the center of each row in a UVIS exposure holds 30 × 2 virtual serial overscan columns. Finally, 19 rows of parallel overscan reside in the inter-chip gap. Fig. 1 depicts this detector format for a raw image of full-chip readout. In EPER mode, however, overscan regions are modified, as shown in Fig. 2. EPER readouts contain 300 pixels of serial overscan and 300 pixels of parallel overscan for each chip. It is the parallel overscan region that is used for CTE analysis. For more information about the configuration of EPER observations, we direct you to Kozhurina-Platais et al. (2011 B).

UVIS CTE Measurements

We continue to perform UVIS EPER CTE measurements and analysis as described by Kozhurina-Platais et al. (2011 B). In short, the CTE is calculated from the ratio of the amount of deferred charge in the extended pixel region (S_D, in e^-) to the product of the charge level of the active science pixels of the last row (S_{LC}, in e^-) and the number of signal transfers of the science pixels in the CCD register (N_P) (Janesick 2001; Eq. 5.21):

$$CTE_{EPER} = 1.0 - \frac{S_D}{S_{LC} \times N_P} \tag{1}$$

where $N_P = 2051$ for WFC3. We average several columns of deferred charge to reduce the noise and increase the signal-to-noise ratio in the extended pixel region. Only the 180 overscan rows closest to the science pixels are measured. Fig. 3 shows a typical signal profile for a single amplifier. Note that the amount of deferred charge decreases with increasing distance from the science pixels (which end at row 301), as it asymptotically approaches the bias level at approximately the 180th row.

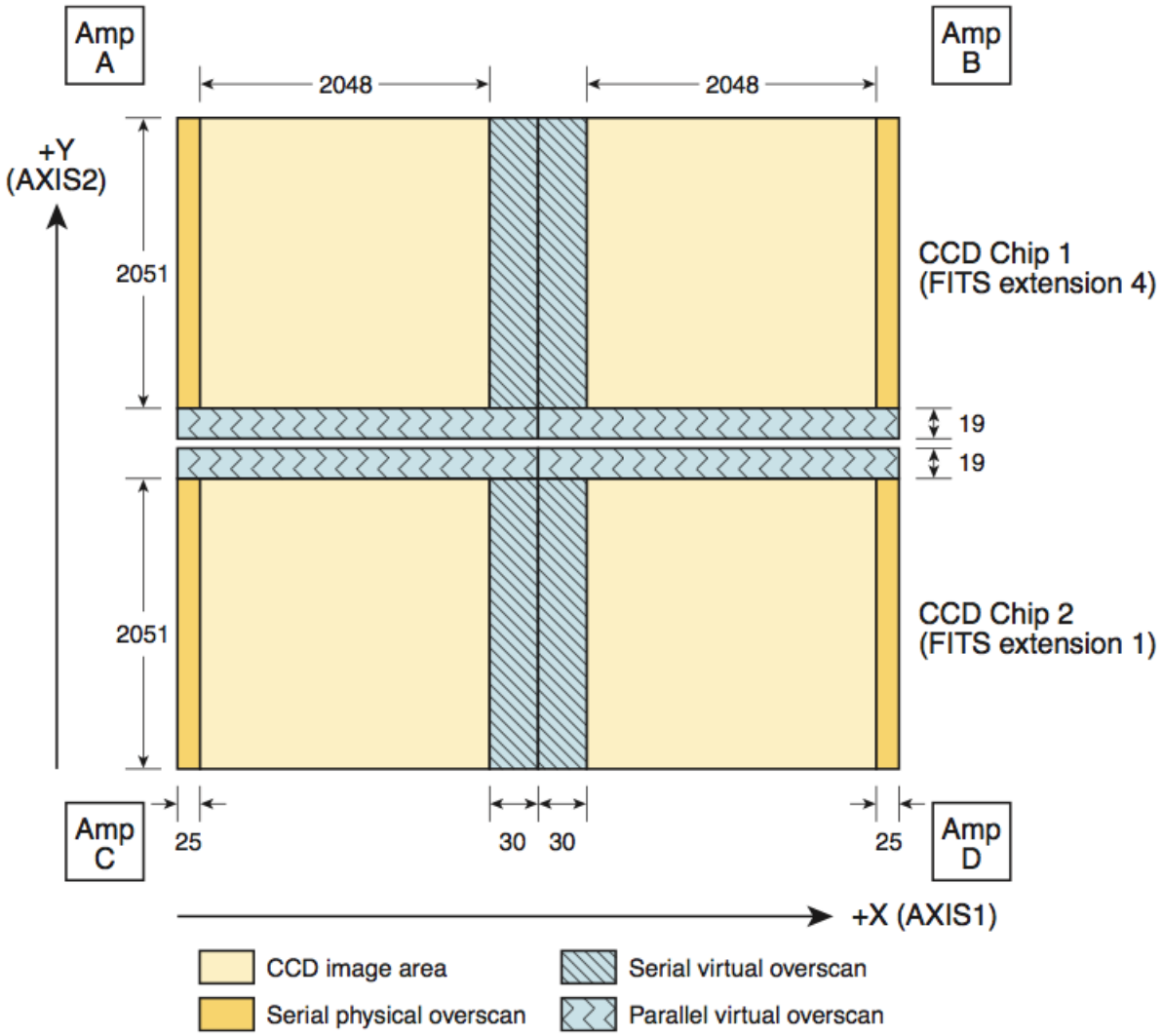

Fig. 1.—*Schematic illustration of a standard WFC3 UVIS image, from Figure 6.14 of the WFC3 Instrument handbook (Dressel, L. (2012)). Science pixels are represented by the light yellow regions, serial physical overscan regions are represented in dark yellow, and serial virtual and parallel virtual ovserscan are represented in blue.*

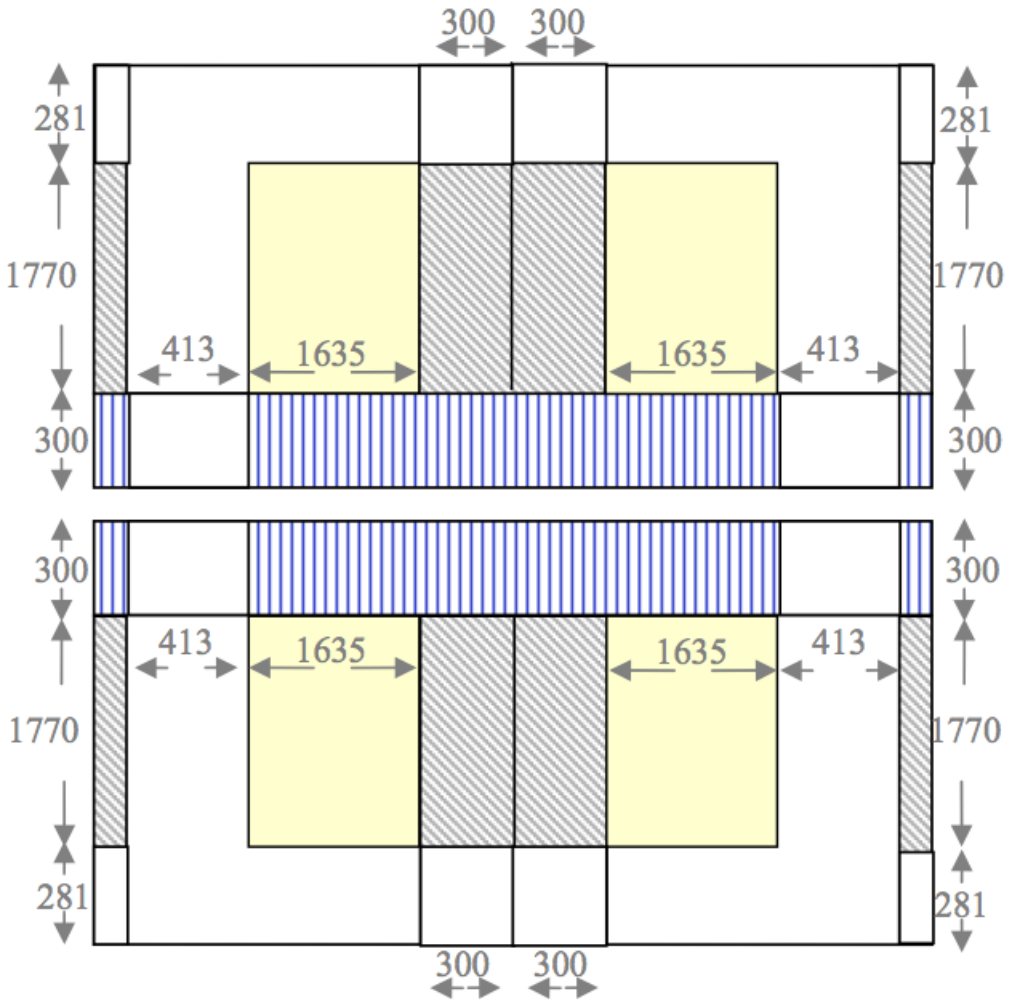

Fig. 2.—*Schematic illustration of an EPER WFC3 UVIS sub-array (Robberto 2007; Figure 2). The CCD image area is represented by yellow. The parallel virtual overscan region is represented with blue stripes and the grey color depicts the serial virtual overscan areas. The white color sections represent areas that are not read out.*

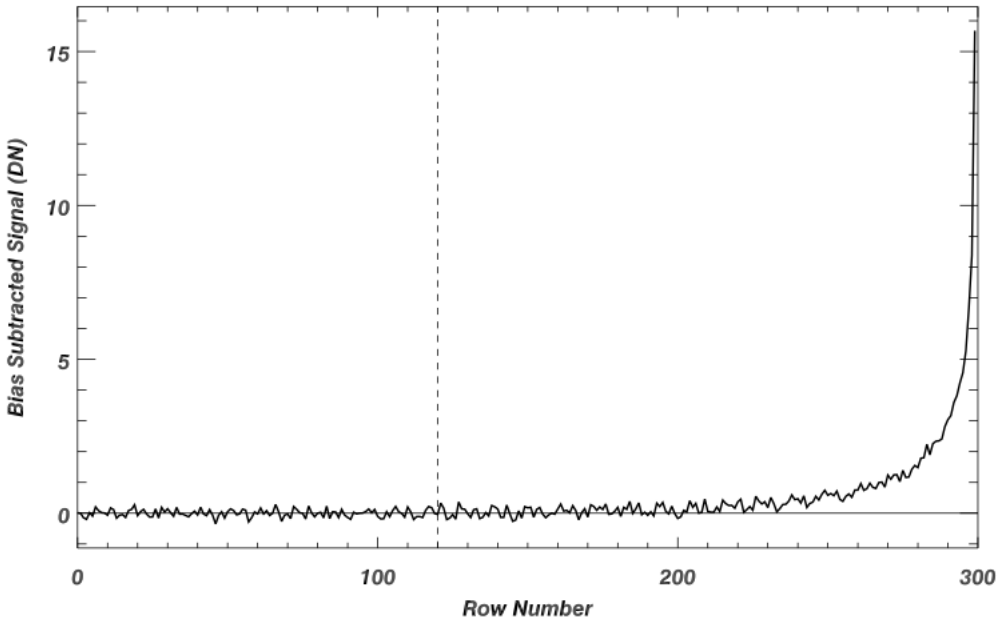

Fig. 3.—*An example of a deferred charge profile from an EPER measurement for amplifier A, from Kozhurina-Platais et al. (2011 B) (Fig. 3). The cutoff position used in the calculation of S_D is represented by the vertical dashed line, meaning that S_D is the sum of the signal in the 180 overscan rows closest to the science pixels.*

Low-level periodic noise continues to be a factor in some EPER observations, affecting both dark and tungsten flat field exposures. This periodic noise, which manifests itself in every 11th row of the image, does not appear in normal imaging mode but rather only in the special EPER readout mode. A super-dark image, which was constructed from individual dark images that do not contain this periodic noise, was used for calibrating the EPER internal flat field images. A sigma-clipping technique was employed to remove the noise from EPER observations that were also affected. Fig. 4 serves as an example of the periodic noise seen in the signal profiles of some EPER observations. Note that the noise component varies in amplitude and sign, but consistently has an 11 row periodicity. The sigma-clipping technique used to filter out this noise is further described in Kozhurina-Platais et al. (2011 B). After noise filtering was performed, the EPER CTE was calculated using Eq. (1).

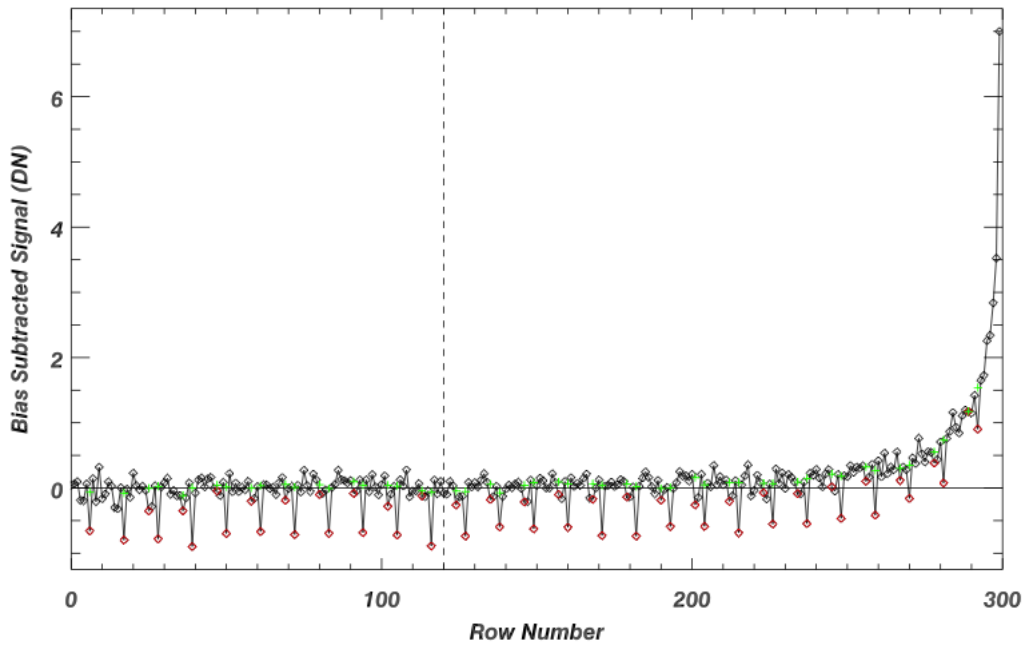

Fig. 4.—*An example of a profile of the deferred charge with periodic noise, from Kozhurina-Platais et al. (2011 B) (Fig. 4). Red symbols indicate the periodic noise and the green symbols show the signal after noise filtering is applied.*

Results

Here we present three plots showing the results of CTE analysis since the first internal WFC3 EPER observation in August, 2009. Fig. 5 shows the EPER CTE versus the signal level of the last row of the active science pixels (S_{LC}) for each individual exposure and for each amplifier. The EPER CTE continues to asymptotically approach 1.0 at the highest signal levels. CTE is greater at higher signal levels because of lower fractional losses.

Fig. 6 details the power-law relationship between the CTE and signal level, as described in Kozhurina-Platais et al. (2011 B):

$$log(CTI) = log(m) + \rho \times log(S_{LC}) \tag{2}$$

where *CTI* is the charge transfer inefficiency (the loss of charge as singal is transferred between pixels; defined here as *1 - CTE_{EPER}*) and *log(m)* and ρ are slope and the intercept of the *log-log CTI*, respectively. The top panel of Fig. 6 contains the CTE measurements for each individual exposure and for all four amplifiers as a function of signal level, with a solid red line as the best linear fit of Eq. (2). We continue to observe similar CTI profiles as those in Cycles 17 and 18. The middle panel, which plots ρ over time with a best linear fit (red line), reveals that the *log-log* slope

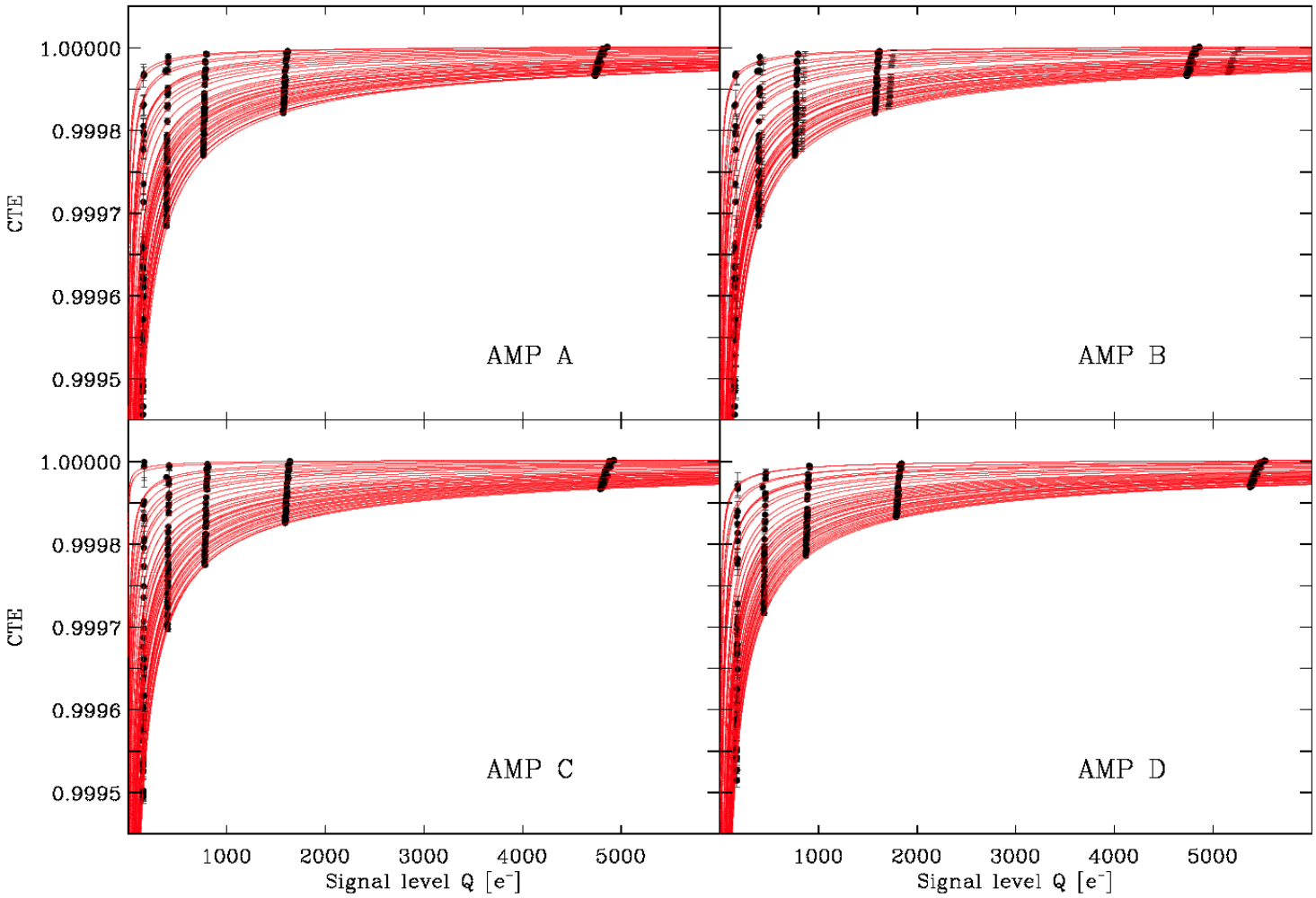

Fig. 5.—*UVIS CTE versus signal level for each individual exposure (black circles) and for each amplifier. Uncertainties were derived from the ratio of the standard deviation of S_D and the denomonator in equation (1). Each over-plotted red line represents the best power-law fit for the particular observation.*

of the CTI versus signal level remains independent of time, as the average value for ρ is ∼-0.68, the same as it was through Cycle 18. It is thought that the ρ parameter is intrinsic to the UVIS CCD and was established during the manufacturing process. The bottom panel plots *log(m)* versus time with a linear best-fit line shown in red. Results show that, with ρ fixed at ∼0.68, the CTI is increasing over time. It should be noted that the parameter m shows less increase in recent EPER measurements (i.e. since 2011; MJD $\gtrsim$ 55.5). It is thought that this slower CTE degradation may be a consequence of changes in solar activity. For example, the South Atlantic Anomaly (SAA) may have been stronger, especially during the 2009-2010 solar minimum, causing more rapid CTI increase (Baggett et al. 2011). The recent increase in solar activity is expected to have lowered the intensity of radiation capable of damaging the detector lattice and decrease the rate of degradation.

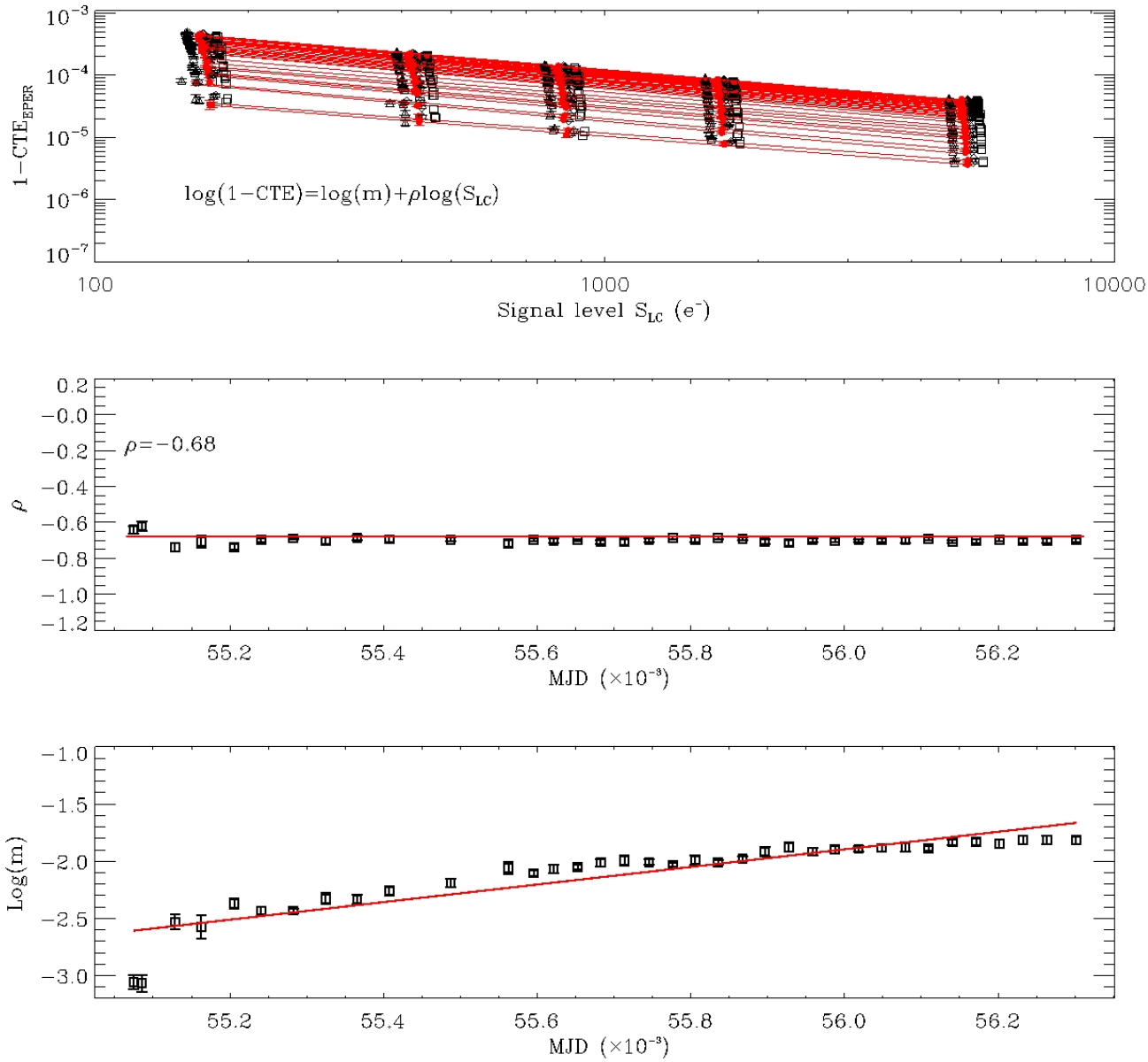

Fig. 6.—*Three plots showing the power law relationship between CTE and signal level. The top panel shows the log-log plot of CTI versus signal level (in* e^-*), with a line of best linear fit for each observation. Asterisk symbols, diamonds, triangles, and squares represent measurements for the four amplifiers, A, B, C, and D, respectively. The middle panel shows the log-log CTI slope (*ρ*) versus time with an over- plotted line of best linear fit. The bottom panel shows the log-log CTI intercept (m) as a function of time, also with a line of best linear fit.*

Fig. 7 shows the UVIS CTE measurements as a function of time for each signal level. We continue to see that CTE declines linearly over time for each signal level and that CTE loss is worst at lowest signal levels.

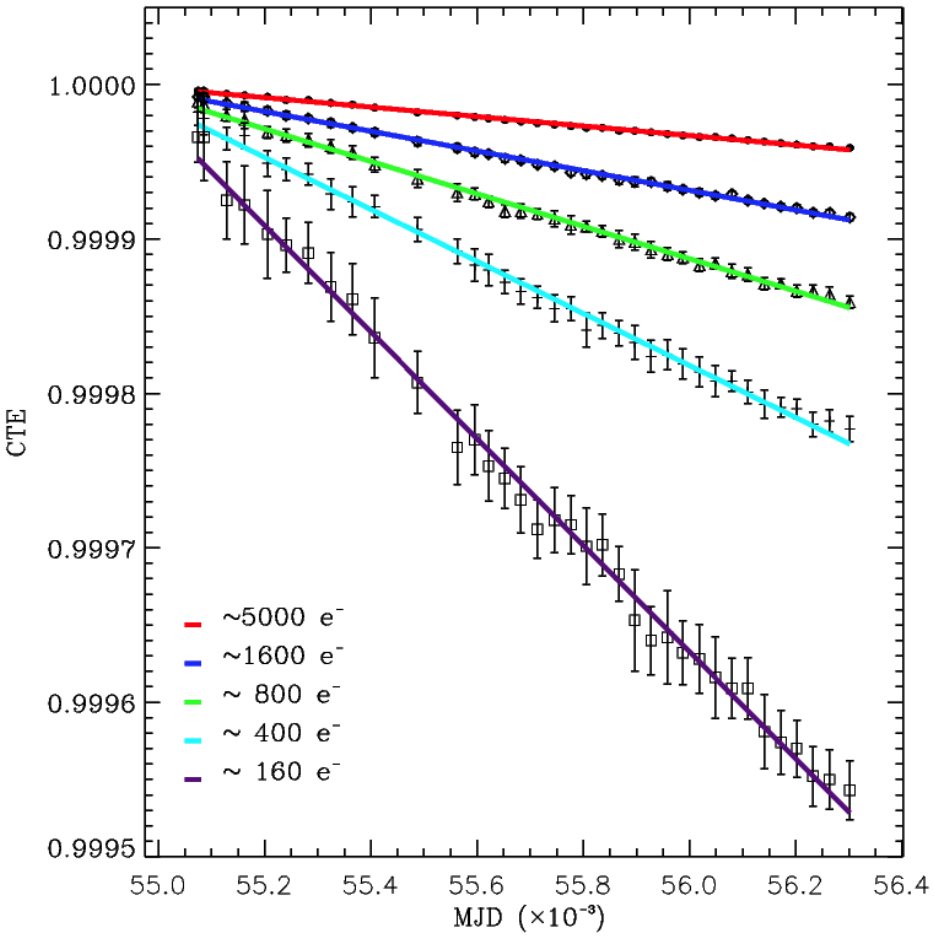

Fig. 7.—*CTE as a function of time for a range of signal levels spanning August 2009 through January 2013. CTE continues to decline linearly over time and decreases most rapidly for the lowest signal level of 160 e^-.*

For further comments on EPER CTE results from observations taken during Cycles 17 and 18, we direct you to Kozhurina-Platais et al. (2011 B).

Conclusion

The EPER method to measure the WFC3/UVIS CTE is an established monitoring program that has been employed since the start of on-flight WFC3 exposures during Cycle 17. The EPER method uses internal exposures to measure the signal in trailing overscan regions to assess the CTE, and thus is an efficient and cost effective way to monitor the WFC3/UVIS CTE over time, as it

avoids using valuable external observing time. However, though EPER measurements are useful for evaluating the CTE degradation performance for a given instrument, a direct correction in stellar photometry or astrometry is not a product of this analysis.

Presented here are WFC3/UVIS EPER CTE measurements through Cycle 19 and including the first three observations of Cycle 20, spanning observations from August 2009 through January 2013. Using the same data analysis techniques as were used in Cycles 17 & 18, we continue to observe the same correlations between CTE, signal level, and time. Namely, the CTE continues to decline linearly over time and decreases the most steeply for lower signal levels. We also observe some evidence for a suppression in detector degradation since MJD $\approx$ 55.5 (October, 2010). EPER CTE monitoring will continue through and perhaps beyond Cycle 20. For latest WFC3/UVIS EPER CTE measurements, please visit www.stsci.edu/hst/wfc3/ins_performance/monitoring/.

Acknowledgements

We would like to thank Sylvia Baggett for her keen interest and support of the WFC3/UVIS EPER CTE project. We also send appreciation to Bryan Hilbert for his help with IDL and the data analysis software, and to Kai Noeske for his thorough review of this ISR.

References

Baggett, S., Bushouse, H., Gilliland, R., Kozhurina-Platais, V., Noeske, K., Petro, L., 2011, in "http://www.stsci.edu/hst/wfc3/ins performance/CTE/CTE.pdf"

Chiaberge, M., Lim, P.M., Kozhurina-Platais, V., Sirianni, M., Mack, J., 2009, ACS Science Instrument Report 2009-01, (Baltimore: STScI)

Dolphin, A. E., 2000, PASP, 112, 1397

Dressel, L., 2012. "Wide Field Camera 3 Instrument Handbook, Version 5.0" (Baltimore: STScI)

Gilliland, R., Goudfrooij, P., Kimble, R., 1999, PASP, 111, 1009

Goudfrooij, P., & Kimble, R. A., 2003, in 2002 HST Calibration Workshop, eds. A. Arribas, A. Koekemoer, & B. C. Whitmore (Baltimore: STScI), p.105

Goudfrooij, P., Bohlin, R. C., & Maíz Apellániz, J., 2006, PASP, 118, 1455

Janesick, J.R., 2001, "Scientific Charge-Coupled Devices", SPIE Press, Bellingham VA

Kozhurina-Platais, V., Goudfroij P., Puzia, T., 2007, ACS Science Instrument Report 2007-04, (Baltimore: STScI)

Kozhurina-Platais, V., Hilbert, B., Martel, A., & McCullough, P., 2009, WFC3 Instrument Science Report 2009-10 (Baltimore, STScI)

Kozhurina-Platais, V., Gilliland, R., & Baggett, S., 2011, WFC3 Instrument Science Report 2011-06 (Baltimore, STScI)

Kozhurina-Platais, V., Hilbert, B., Baggett, S., & Petro, L., 2011, WFC3 Instrument Science Report 2011-17 (Baltimore, STScI)

Mutchler, M., & Sirianni, M., 2005, ACS Instrument Science Report 2005-03 (Baltimore: STScI)

Noeske, K., Baggett, S., Bushouse, H., & Petro, L., 2012, WFC3 Instrument Science Report 2012-09 (Baltimore, STScI)

Riess, A., 2003, ACS Science Instrument Report 2003-09 (Baltimore: STScI)

Riess, A., & Mack, J., 2004, ACS Science Instrument Report 2004-06 (Baltimore: STScI)

Robberto, M., 2007, WFC3 Instrument Science Report 2007-13 (Baltimore: STScI)

Whitmore, B. C., Heyer, I., & Casertano, S., 1999, PASP, 111, 1539